Nonlinear influence of excess Mn on the magnetoelastic transition in (Mn,Cr)$_2$Sb

Shen, Qi; Batashev, Ivan; Ojiyed, Hamutu; Zhang, Fengqi; van Dijk, Niels; Brück, Ekkes

Important note
To cite this publication, please use the final published version (if applicable).
Please check the document version above.

Research Article

Nonlinear influence of excess Mn on the magnetoelastic transition in $(Mn,Cr)_2Sb$

Qi Shen*, Ivan Batashev, Hamutu Ojiyed, Fengqi Zhang, Niels van Dijk, Ekkes Brück

Fundamental Aspects of Materials and Energy, Faculty of Applied Sciences, Delft University of Technology, Mekelweg 15, 2629 JB Delft, The Netherlands

ABSTRACT

The influence of excess Mn on the magnetoelastic ferromagnetic-to-antiferromagnetic transition T_t in the magnetocaloric compound $(Mn,Cr)_2Sb$ has been studied. With increasing excess Mn the magnetoelastic transition temperature for $(Mn,Cr)_2Sb$ initially increases and then decreases. This trend is accompanied by a strong reduction of the $(Mn,Cr)Sb$ secondary phase. With increasing excess Mn a higher Cr content was found in the $(Mn,Cr)Sb$ secondary phase in comparison to the matrix phase. This competition for Cr leads to a nonlinear dependence of T_t with increasing excess Mn at a fixed nominal Cr content. However, we observed that T_t depends linear on the c/a ratio for a wide range of temperatures from 170 to 350 K. A compositional diagram of the c/a ratio was constructed to assist the selection of $(Mn,Cr)_2Sb$ alloys with a desired transition temperature.

1. Introduction

The magnetocaloric effect (MCE), associated with either an isothermal entropy change or an adiabatic temperature change in the presence of a change in magnetic field, can be used for magnetic refrigeration and waste heat recovery [1,2]. A tunable transition temperature and a narrow thermal hysteresis are two basic requirements of promising magnetocaloric materials for these two environmentally friendly applications [3,4]. In recent years Mn_2Sb-based alloys undergoing a first-order magnetoelastic transition (FOMT) from a ferrimagnetic state to an antiferromagnetic state (FIM-AFM) at critical temperature T_t attract increasing attention [5–7]. The FOMT has been studied in many Mn_2Sb-based compounds with elemental substitution such as V [8], Cr [5], Zn [9], Co [10] on the Mn sites or Sn [11], As [12], Ge[13], Bi [14,15] on the Sb site. Among these compounds, Cr-doped Mn_2Sb is one of the most promising magnetocaloric candidate materials with a wide range of FOMT temperatures ranging from 220 to 340 K, a narrow thermal hysteresis (less than 2 K), a large inverse magnetocaloric entropy change of 7.5 J/kg K [5] and an adiabatic temperature change of 2 K under a field change of 5 T [7]. The $(Mn,Cr)_2Sb$ compounds have a tetragonal Cu_2Sb-type crystal structure and order ferrimagnetically below a transition temperature (T_C) of 550 K. The Mn atoms occupy two different crystallographic sites: Mn-I ($2a$) with a magnetic

moment of 2.1 μ_B and Mn-II ($2c$) with a magnetic moment of 3.9 μ_B [16]. Along the c axis the Mn-I and Mn-II moments align parallel or antiparallel to each other between layers corresponding to the ferrimagnetic or the antiferromagnetic structure, respectively. The FIM-AFM transition finds its origin in the chemical compression introduced by smaller atom substitutions for Mn or Sb in the typical case of $(Mn,Cr)_2Sb$ [5,17] or by enhanced thermal expansion in the case of $Mn_2(Sb,Bi)$ [14,18]. Upon cooling, the lattice parameter c of the $(Mn,Cr)_2Sb$ compounds decreases below a critical value, resulting in an exchange inversion for adjacent Mn-II and Mn-II moments, accompanied by a large magnetisation jump at the FIM-AFM transition [17].

In the $(Mn,Cr)_2Sb$ compounds the FIM-AFM magnetisation jump is generally reduced by the presence of a MnSb-type impurity phase. MnSb is a ferromagnet with a Curie temperature of $T_C = 588$ K. The unavoidable MnSb impurity is related to an instability of the Mn_2Sb main phase below 900 K [19]. The evaporation of Mn enhances the tendency towards the non-stoichiometric Mn-deficient side. Therefore, a small amount of excess Mn is added during the arc-melting process to compensate for the evaporation of Mn [15,20,21]. However, some residual Mn (beyond the amount of compensating for evaporation) easily remains in the samples [21], which may influence the chemical composition and the FOMT transition of the main phase due to the large magnetic moment of Mn atoms in Mn_2Sb-based alloys. We find from our study adding different amount of excess Mn, that in order to obtain the desired $(Mn,Cr)_2Sb$ alloys with large step in magnetisation for magnetocaloric applications, it is

---

* Corresponding author.
  E-mail address: q.shen@tudelft.nl (Q. Shen).

Table 1
Main-phase composition (in at%) determined by EDS for the $(Mn,Cr)_2Sb$ alloys.

	Cr1Mn0	Cr1Mn2	Cr1Mn8	Cr2Mn0	Cr2Mn2	Cr2Mn8	Cr3Mn0	Cr3Mn2	Cr4Mn0	Cr4Mn2	Cr5Mn2	Cr5Mn8	Cr6Mn2
Cr	1.1	1.1	1.1	1.2	1.7	1.3	2.2	1.7	2.6	2.7	2.9	2.3	3.6
Mn	64.6	64.8	65.1	64.2	63.7	64.4	63.2	64.3	63.5	62.6	62.5	62.9	61.5
Sb	34.3	34.1	33.7	34.6	34.6	34.3	34.6	34.0	33.9	34.7	34.6	34.8	35.0

very important to study the properties of nonstoichiometric $(Mn,Cr)_2Sb$ alloys. Therefore, we investigated in this paper the influence of excess Mn on the magnetoelastic transition and magnetocaloric effect in $(Mn,Cr)_2Sb$ compounds with an excess 0, 2 and 8 wt% Mn.

2. Experimental methods

Thirteen polycrystalline $(Mn,Cr)_2Sb$ compounds with an excess 0, 2 and 8 wt% Mn were prepared from high-purity elements (Mn 99.9%, Cr 99.995%, Sb 99.5%) by arc melting. The starting compositions are indicated as CrxMny, where x and y correspond to the nominal Cr content and excess Mn in wt%, respectively. The arc-melted samples were annealed for homogenisation under argon atmosphere at 1073 K for 5 days. The compositions of the resulting alloys given in Table 1 were determined by the Energy Dispersive X-ray Spectroscopy (EDS). X-ray diffraction (XRD) data were collected with a Panalytical X-Pert PRO using Cu-K$_\alpha$ radiation. The lattice constants were analysed by Rietveld refinement using Fullprof [22]. The microstructure was analysed by Electron Probe Micro Analysis (EPMA) model JEOL JXA 8900R equipped with the Wavelength Dispersive Spectrometry (WDS) and the Scanning Electron Microscopy (SEM) model FEI Quanta FEG 450 equipped with the EDS. The magnetic properties in the temperature range of 5–370 K were measured on a superconducting quantum interference device (SQUID) magnetometer model MPMS-XL, equipped with the reciprocating sample option. The high-temperature magnetic measurements in the range 315–600 K were carried out using a vibrating sample magnetometer (VSM) model LakeShore 7307 equipped with a high-temperature oven (Model 73034). T_C is obtained from the maximum absolute temperature derivative of the magnetisation $|dM/dT|$ in the heating curve under a magnetic field of 0.01 T. The transition temperature T_t is determined from the corresponding temperature of maximal value of dM/dT under a magnetic field of 1 T, to avoid interference with the spin reorientation effect that is present in low magnetic fields.

3. Results and discussion

Fig. 1(a) and (b) show the XRD data at room temperature for the Cr2Mny (y = 0, 2, 8 wt%) samples (nominal 2.7 wt% Cr) and the CrxMn2 (x = 1, 2, 3, 4, 5, 6 wt%) samples (nominal excess 2 wt% Mn), respectively. The main phase is identified as the tetragonal CuSb-type $(Mn,Cr)_2Sb$. The XRD patterns show a preferred orientation signalled by the enhanced (00l) reflections in all samples, which have also be observed in Cr-modified Mn_2Sb [5] and in Co-modified Mn_2Sb [10]. Besides the main phase, the peaks around 29° and 40° indicate the hexagonal impurity phase $(Mn,Cr)Sb$. The fraction of secondary phase is given by SEM images instead of XRD refinement because of the preferred orientation. The $(Mn,Cr)Sb$ peaks show a strong decrease in intensity with increasing excess Mn in Fig. 1(a), whereas an increase is observed with increasing Cr substitution in Fig. 1(b). Excess Mn is found to suppress the Mn-deficient tendency [20], but increasing Cr enhances this tendency since Cr occupies the Mn-I site, as determined by neutron diffraction [23]. As shown in Fig. S1 in the Supplementary material, adding excess Mn reduces the fraction of secondary phase in low-Cr content samples, but has limited contribution to reducing the fraction of secondary phase in

high-Cr content samples. The lattice parameters c (6.5369 Å for Cr2Mn0, 6.5364 Å for Cr2Mn2, 6.5377 Å for Cr2Mn8) and the c/a ratio (1.6027 for Cr2Mn0, 1.6022 for Cr2Mn2, 1.6033 for Cr2Mn8) initially decrease with 2 wt% excess Mn and then increase with 8 wt% excess Mn, displaying the same trend as the unit-cell volume of the main phase, as shown in Fig. 1(c). With the increase in excess Mn, the enhanced unit-cell volume of the main phase indicates that 2 wt% of excess Mn enters Mn voids caused by the Mn-deficient tendency of Mn_2Sb phase [20]. When the excess Mn increases up to 4 wt%, the unit-cell volume of the main phase starts to decrease, suggesting that the additional Mn (beyond 2 wt%) replaces Sb due to the smaller atom size of Mn compared to Sb. Meanwhile, due to the smaller atom size of Cr compared to Mn, the trend of a decreasing unit-cell volume for $(Mn,Cr)Sb$ in Fig. 1(d) implies an increase in Cr content in the $(Mn,Cr)Sb$ secondary phase.

The back-scattered SEM images of the Cr2Mn0, Cr2Mn2 and Cr2Mn8 samples are shown in Fig. 2(a–c). The white area and the black spots are determined by EDS to be secondary $(Mn,Cr)Sb$ and Mn phases, respectively. The volume fraction of the secondary phases shows a sharp decrease with increasing excess Mn: 10% for Cr2Mn0, 4% for Cr2Mn2 and 1% for Cr2Mn8 (obtained by image analysis with the software package ImageJ). The absence of the Mn phase in the XRD patterns can be attributed to the fact that the amount is too small to be detected. The cracks observed for the Cr2Mn0 and Cr2Mn2 samples are probably caused by the difference in thermal expansion for the $(Mn,Cr)_2Sb$ and $(Mn,Cr)Sb$ phases. Table 1 gives the chemical compositions of the $(Mn,Cr)_2Sb$ alloys determined by EDS. Generally, the content of Cr in $(Mn,Cr)_2Sb$ increases with the increasing nominal Cr content and the increasing nominal excess Mn content. The content of Cr fluctuates for the different amounts of excess Mn, except for Cr1Mny (y = 0, 2, 8) samples, which have ultra-low Cr contents. The same Cr content in the main phase for Cr2Mn2 and Cr3Mn2 can be ascribed to the fact that the latter has more $(Mn,Cr)Sb$ secondary phase, as indicated in XRD patterns in Fig. 1(b). Compared with the CrxMn2 samples (x = 2, 5), the CrxMn8 samples (x = 2, 5) tend to have lower Cr contents, which indicates that too much excess Mn expels Cr from the main phase to the secondary phases. The chemical composition of the Cr1Mn8 sample was also confirmed by WDS to be $Mn_{62.7}Sb_{35.9}Cr_{1.4}$ obtained from the average of 19 points, which is slightly different from $Mn_{65.1}Sb_{33.7}Cr_{1.1}$ determined by EDS. The elemental composition variation for $(Mn,Cr)Sb$ and $(Mn,Cr)_2Sb$ can be compared from the line scans by WDS for the Cr1Mn2 sample in Fig. 2(d). We found 1.8 at% Cr in the $(Mn,Cr)Sb$ secondary phase and 1.4% at% Cr in the main phase, which indicates the preference of Cr for the $(Mn,Cr)Sb$ secondary phase.

Fig. 3(a–b) display the M-T curves for the Cr2Mny (y = 0, 2, 8). Upon cooling, a sharp magnetisation jump at T_t in Fig. 3(a) almost free of hysteresis reflects the magnetoelastic FIM-AFM transition. For the Cr2Mn0 sample, the broad transition and the high residual magnetisation below T_t can be accounted by the large fraction of about 10% $(Mn,Cr)Sb$ secondary phase obtained from the SEM image. Compared with the Cr2Mn8 sample, the Cr2Mn2 sample shows a 30 K higher T_t. Similarly, the Cr1Mn2 sample shows a 20 K higher T_t than the Cr1Mn0 and Cr1Mn8 samples (see Fig. S2 in the Supplementary material). Although Cr1Mn4 has a higher T_t than Cr1Mn2, the larger fraction of $(Mn,Cr)Sb$, indicated from the higher residual magnetisation below T_t, makes the magnetisation jump
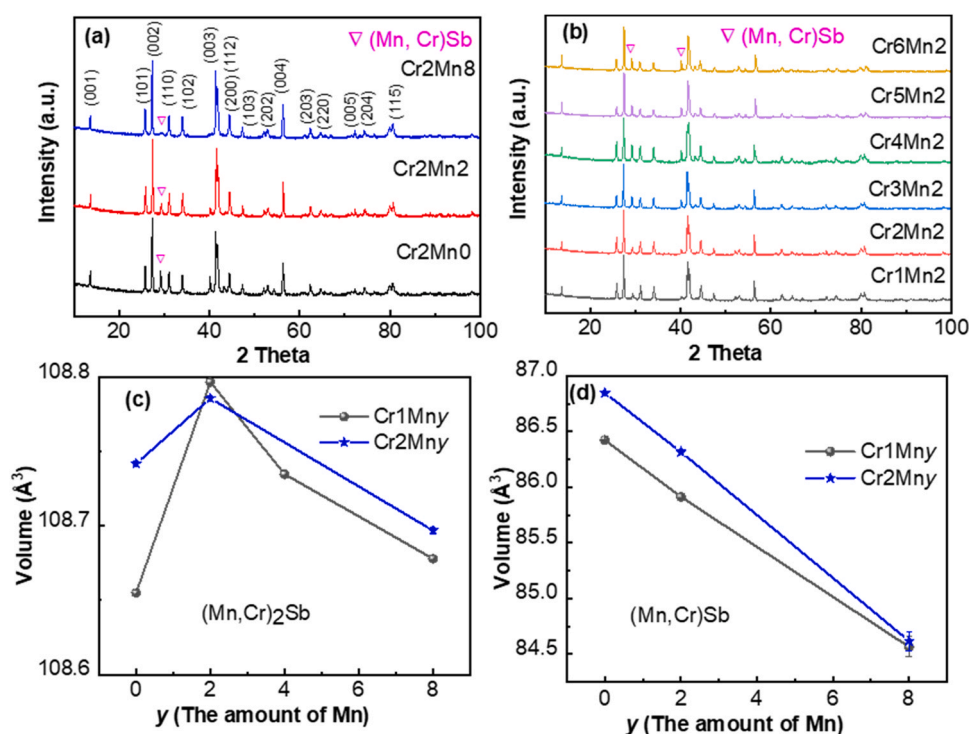
Fig. 1. XRD patterns for (a) Cr2Mny samples (y = 0, 2, 8) (b) CrxMn2 samples (x = 1–6). Excess Mn content dependence of the unit-cell volume (c) for the (Mn,Cr)$_2$Sb main phase and (d) for the (Mn,Cr)Sb secondary phase.

smaller for the former than for the latter. The T_C presented in Fig. 3(b) shows a slightly decrease with the increase in excess Mn: T_C = 535 K for Cr2Mn0; T_C = 528 K for Cr2Mn2 and T_C = 527 K for Cr2Mn8.

Consequently, using 2 wt% excess Mn can help to obtain more pure sample with a higher transition temperature. Fig. 3(c) shows

the M-T curves for the CrxMn2 (x = 1–6) samples. Substitution with the smaller element Cr for Mn causes the contraction of the unit cell and thus strengthens the antiferromagnetic interaction between the Mn-I and Mn-II moments [24]. Therefore, the transition temperature T_t shifts to higher temperature with increasing nominal Cr contents except for the Cr3Mn2 sample. The reduction in the magnetisation
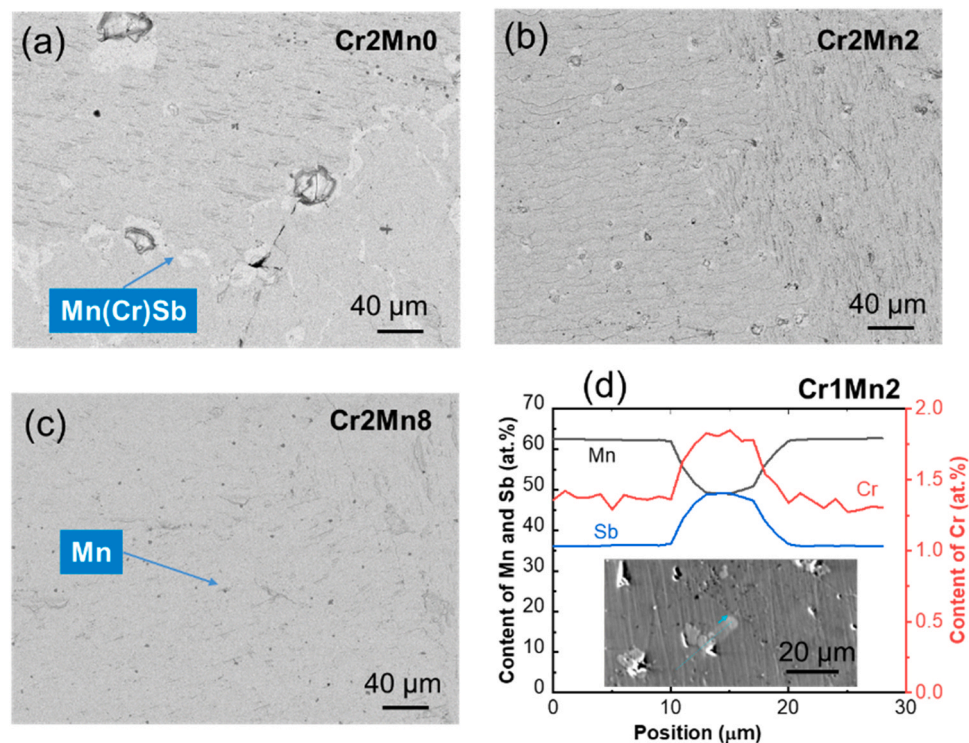

Fig. 2. (a–c) Back-scattered SEM images for the Cr2Mny (y = 0, 2, 8) samples. (d) Line scans through the white secondary phase in the inserted EPMA images for the Cr1Mn2 sample.
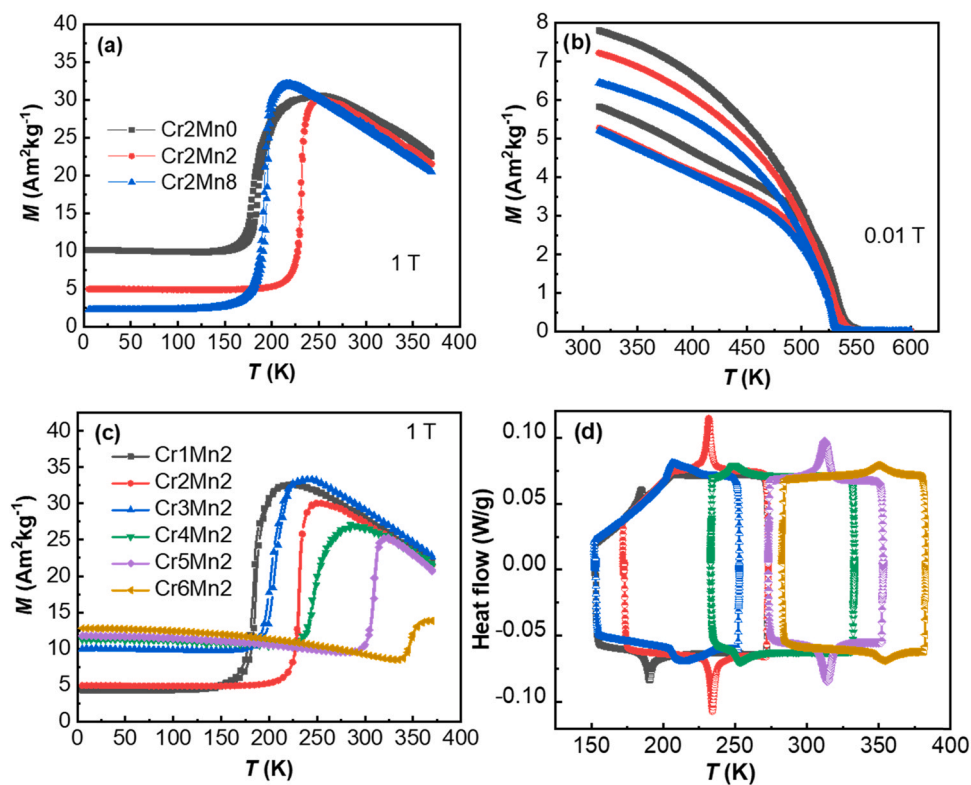
Fig. 3. *M-T* curves of Cr2Mn*y* (*y* = 0, 2, 8) in a temperature range of (a) 5–370 K and (b) 315–600 K. (c) *M-T* curves (d) DSC curves for Cr*x*Mn2 (*x* = 1–6) samples.
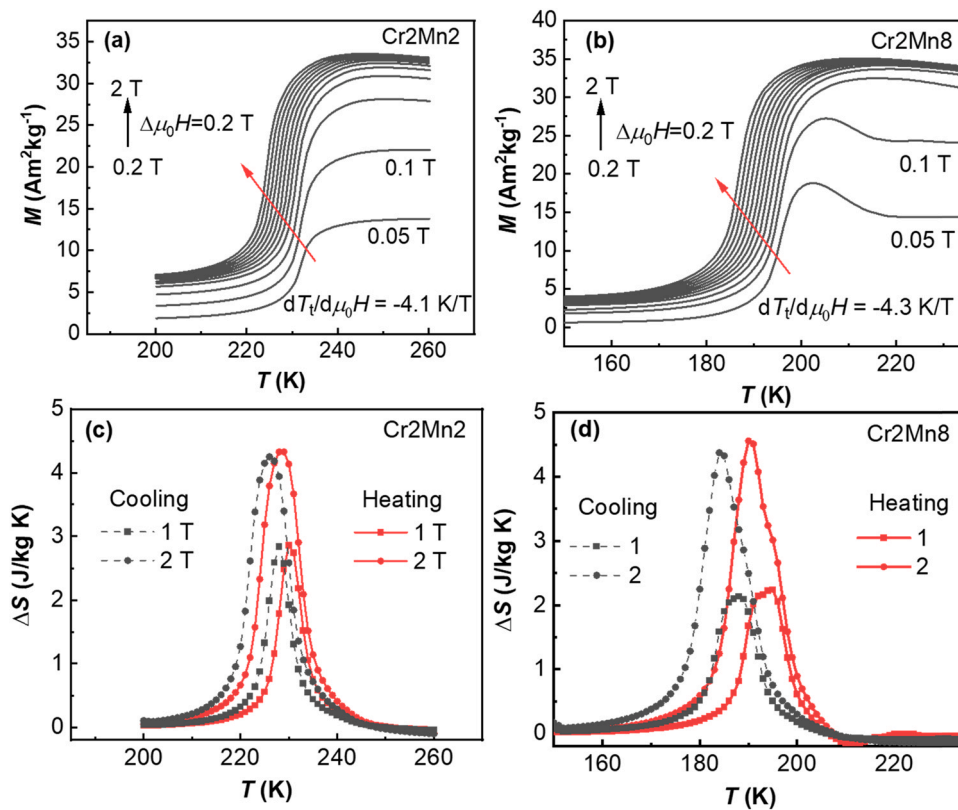

Fig. 4. *M-T* curves upon heating in different magnetic fields for (a) Cr2Mn2 and (b) Cr2Mn8. The magnetic entropy change calculated from heating and cooling curves for (c) Cr2Mn2 and (d) Cr2Mn8.
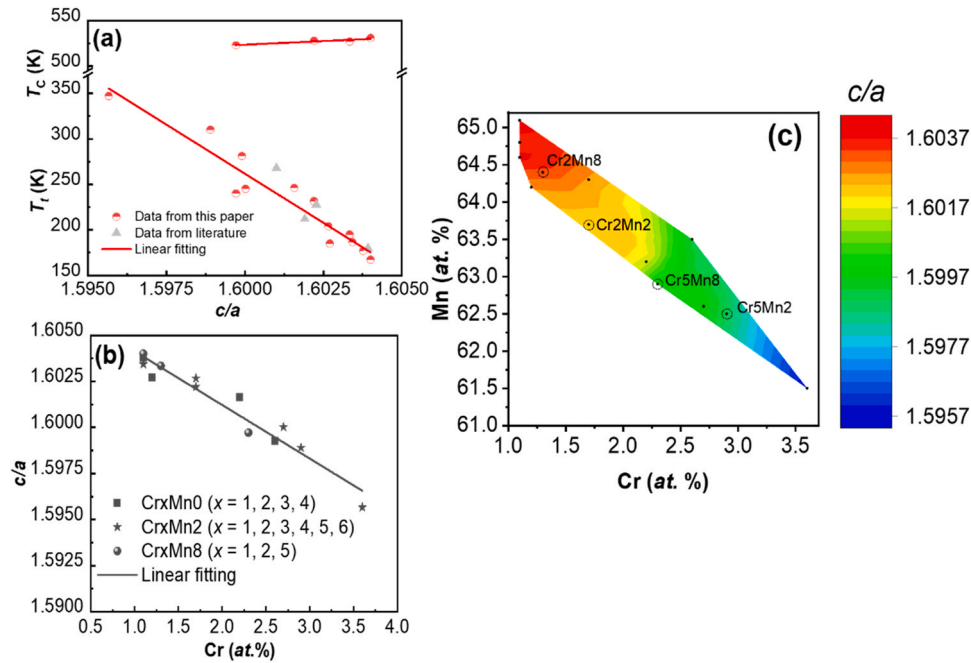
Fig. 5. (a) T_t and T_C as a function of the c/a lattice parameter ratio. Grey data points are from literature [5,21,25]. (b) The ratio of c/a lattice parameter dependence of Cr concentration determined by EDS. (c) Composition for the $(Mn,Cr)_2Sb$ compounds as a function of the c/a lattice parameter ratio. The black points correspond to the experimental data. All data are measured in the ferrimagnetic state.

jump with increasing Cr addition corresponds to the increased fraction of (Mn,Cr)Sb. A higher Cr addition supports the tendency towards the Mn-deficient side and inevitably induces more (Mn,Cr) Sb secondary phase. The large exothermal and endothermal peaks depicted in DSC curves in Fig. 3(c) reflect the nature of the FOMT for CrxMn2 ($x = 1$–6) samples. A similar increasing tendency of the transition temperature with increasing Cr addition (and the abnormal T_t for the Cr3Mn2 sample) are also observed from the DSC curves, in agreement with the M-T curves. The latent heat determined from the heating curve for the Cr2Mn2 sample amounts to 1.2 J/g, and the estimated entropy change of about 5.3 J/kg K in the absence of an external magnetic field is close to the value of 5.1 J/ kg K reported for $Mn_{1.94}Cr_{0.06}Sb$ [5].

The magnetic entropy changes for the Cr2Mn2 and Cr2Mn8 samples have also been calculated from temperature-dependent magnetisation at variable fields as shown in Fig. 4. A higher magnetic field stabilises the FIM state and shifts the transition temperature to a lower temperature. The magnetic field dependence of the transition temperature for Cr2Mn2 and Cr2Mn8 is − 4.1 K/T and − 4.3 K/T, respectively. For Cr2Mn8, the decrease of magnetisation under low magnetic fields around 200 K is due to the spin reorientation effect [21], which is also observed in our previous work on $Mn_2Sb_{1-x}Bi_x$ [14]. The critical magnetic field for this spin-flipping transition is 0.2 T. The entropy change in Fig. 4(c) and (d) is calculated based on the integrated Maxwell relation: $\Delta S(\Delta H, T) = \int_{H_0}^{H} \left(\frac{\partial M(T,H)}{\partial T} \right)_H d\mu_0 H$, where we choose $\mu_0 H_0 = 0$ T. Due to the narrow transitional hysteresis, the magnetic entropy change derived from cooling curves is essentially the same as that derived from heating curves for both samples. Under a magnetic field change of 2 T, the maximal entropy change in the heating curves is 4.3 J/kg K at 228 K for Cr2Mn2 and 4.6 J/kg K at 190 K for Cr2Mn8 sample, which are similar values as those reported in the literature [5,7]. Therefore, the amount of excess Mn can shift the working temperature to a lower temperature without sacrificing the magnetic entropy change.

The evolution of T_t with increasing Cr and excess Mn contents can be explained by the linear relation between T_t and c/a, as

displayed in Fig. 5(a–c). Compared with T_C, the transition temperature T_t is much more sensitive to the c/a ratio. In Fig. 5(a), the grey data points obtained from literature [5,21,25] are approximately in line with the linear trend. Furthermore, the c/a ratio shows a linear dependence on the Cr concentration in the main phase as depicted in Fig. 5(b). A larger c/a ratio for Cr3Mn2 (1.6027) than Cr2Mn2 (1.6022) results in a lower T_t for Cr3Mn2, which can be ascribed to the competition for Cr between the secondary phase and the main phase, as indicated by the same amount of Cr 1.7 at% determined by the EDS for Cr3Mn2 and Cr2Mn2 main phases. In order to further illustrate the relation between chemical composition and T_t, the relation between chemical composition and c/a is displayed in Fig. 5(c). The smallest c/a ratio corresponds to the highest T_t in the high-Cr and low-Mn region, as seen from the higher T_t in CrxMn2 samples ($x = 2$, 5) than CrxMn8 samples ($x = 2$, 5). Since too much excess Mn expels Cr from the main phase to the secondary phases, one should be cautious to add excess Mn when preparing arc-melted $(Mn,Cr)_2Sb$ samples. With the linear relation between T_t and c/a, and the chemical composition diagram, we can now easily tune the desired transition temperature for the Cr-doped Mn_2Sb compounds.

4. Conclusions

The influence of excess Mn on the magnetoelastic transition of $(Mn,Cr)_2Sb$ has been investigated in this work. The fraction of the (Mn,Cr)Sb secondary phase strongly reduces with increasing excess Mn, while the magnetoelastic transition temperature initially increases and then decreases with excess Mn. By Electron Probe Micro Analysis we find that with increasing excess Mn a higher Cr content is found in the (Mn,Cr)Sb secondary phase in comparison to the matrix. This competition for Cr leads to the nonlinear influence of excess Mn on the magnetoelastic transition temperature. However, we observed that T_t scales linear with the c/a lattice parameter ratio for a wide temperature range of 170–350 K. A large magnetic entropy change of 4.6 J/kg K under 2 T is obtained and a composition diagram for the c/a ratio is established to give guidance in the preparation of

(Mn,Cr)$_2$Sb alloys with a desired transition temperature for magnetocaloric applications.

CRediT authorship contribution statement

Qi Shen: Conceptualization, Methodology, Formal analysis, Investigation, Writing – original draft, Writing – review & editing. **Ivan Batashev:** Software, Discussion. **Hamutu Ojiyed:** Methodology, Discussion. **Fengqi Zhang:** Methodology. **Niels van Dijk:** Supervision, Writing – review & editing. **Ekkes Brück:** Supervision, Writing – review & editing.

Declaration of Competing Interest

The authors declare that they have no known competing financial interests or personal relationships that could have appeared to influence the work reported in this paper.

Acknowledgements

Appendix A. Supporting information

Supplementary data associated with this article can be found in the online version at doi:10.1016/j.jallcom.2022.164011.

References

[1] O. Gutfleisch, M.A. Willard, E. Bruck, C.H. Chen, S.G. Sankar, J.P. Liu, Magnetic materials and devices for the 21st century: stronger, lighter, and more energy efficient, Adv. Mater. 23 (2011) 821–842.

[2] S.M. Sandoval, K.P. Wetzlar, G.P. Carman, Thermomagnetic conversion efficiencies for ferromagnetic materials, J. Appl. Phys. 110 (2011) 123923.

[3] N.H. Dung, Z.Q. Ou, L. Caron, L. Zhang, D.T.C. Thanh, G.A. de Wijs, R.A. de Groot, K.H.J. Buschow, E. Brück, Mixed magnetism for refrigeration and energy conversion, Adv. Energy Mater. 1 (2011) 1215–1219.

[4] F. Guillou, G. Porcari, H. Yibole, N. van Dijk, E. Bruck, Taming the first-order transition in giant magnetocaloric materials, Adv. Mater. 26 (2014) 2671–2675.

[5] L. Caron, X.F. Miao, J.C.P. Klaasse, S. Gama, E. Brück, Tuning the giant inverse magnetocaloric effect in Mn$_{2-x}$Cr$_x$Sb compounds, Appl. Phys. Lett. 103 (2013) 112404.

[6] F. Cheng, S. Ma, Y. Wang, X. Ke, J. Wang, S. Yang, Tuning magnetocaloric effect of a Mn-Cr-Sb-Ga alloy by the nonvolatile residual strain of a Ti-Ni shape memory alloy, Acta Mater. 210 (2021) 116849.

[7] A. Tekgül, M. Acet, F. Scheibel, M. Farle, N. Ünal, The reversibility of the inverse magnetocaloric effect in Mn$_{2-x}$Cr$_x$Sb$_{0.95}$Ga$_{0.05}$, Acta Mater. 124 (2017) 93–99.

[8] W. Cui, W.-J. Ren, Z.D. Zhang, X. Zhou, H. Zhong, Q. Wang, Lattice distortion tuning of the metamagnetic phase transition in tetragonal Cu$_2$Sb-type Mn$_{1.95}$V$_{0.05}$Sb alloy, Scr. Mater. 143 (2018) 59–62.

[9] V.I. Val'kov, A.V. Golovchan, I.F. Bribanov, V.I. Kamenev, O.O. Iesenchuk, A.P. Sivachenko, N.N. Kabdin, Stability characteristics of the low temperature ferrimagnetism in the Mn$_{2-x}$Zn$_x$Sb system, Low Temp. Phys. 33 (2007) 70–78.

[10] J. Wilden, A. Hoser, M. Chikovani, J. Perßon, J. Voigt, K. Friese, A. Grzechnik, Co-Magnetic transitions in the Co-modified Mn$_2$Sb system, Inorganics 6 (2018) 113.

[11] V.M. Ryzhkovskii, V.P. Dymont, Z.L. Erofeen, Ferromagnetic-antiferromagnetic phase transition in Mn$_2$Sb(Sn) solid solutions, Phys. Stat. Sol. A 130 (1992) 163–168.

[12] T. Kakimoto, J. Goto, S. Fujii, K. Koyama, S. Ishida, Electronic and magnetic properties of Mn$_2$Sb $_{1-x}$ As $_x$ (x = 0, 0.5, 1), Mater. Trans. 55 (2014) 1878–1884.

[13] J. Zhang, G. Yao, S. Chen, F. Wei, X. Fan, X. Yin, Z. Chen, W. Cui, Q. Wang, The effects of Ge occupation and hydrostatic pressure on the metamagnetic phase transition and magnetocaloric effect in Mn$_2$Sb alloy, AIP Adv. 9 (2019) 035106.

[14] Q. Shen, I. Batashev, F. Zhang, H. Ojiyed, N. van Dijk, E. Brück, The anti-ferromagnetic to ferrimagnetic phase transition in Mn$_2$Sb$_{1-x}$Bi$_x$ compounds, J. Alloy. Compd. 866 (2021) 158963.

[15] Z. Zhang, Y. Zhang, X. Luo, S. Ma, H. Zeng, G. Yu, X. Zheng, C. Chen, Y. Hu, F. Xu, S.U. Rehman, Z. Zhong, Self-organized Bi-rich grain boundary precipitates for realizing steep magnetic-field-driven metamagnetic transition in Bi-doped Mn$_2$Sb, Acta Mater. 200 (2020) 835–847.

[16] M.K. Wilkinson, N.S. Gingrich, C.G. Shull, The magnetic structure of Mn$_2$Sb, J. Phys. Chem. Solids 2 (1957) 289–300.

[17] C. Kittel, Model of exchange-inversion magnetization, Phys. Rev. 120 (1960) 335–342.

[18] K. Shirakawa, H. Ido, Magnetic transition of intermetallic compounds Mn$_2$Sb$_{(1-x)}$Bi$_x$ (0 ≤ x ≤ 0.175) with Cu$_2$Sb type structure, J. Jpn. Inst. Met. 43 (1979) 636–639.

[19] N. Erick, G. Fredrik, The Mn$_2$Sb phase composition and thermodynamic properties in the range 298–1000 K, J. Chem. Therm. 1 (1969) 153–167.

[20] T.J. Swoboda, W.H. Cloud, T.A. Bither, M.S. Sadler, H.S. Jarrett, Evidence for an antiferromagnetic-ferrimagnetic transition in Cr-modified Mn$_2$Sb, Phys. Rev. Lett. 4 (1960) 509–511.

[21] Y. Cao, K. Xu, Z. Li, Y. Zhang, X. He, Y. Kang, W. Sun, T. Gao, Z. Qian, C. Liu, M. Ye, C. Jing, Interplay between spin reorientation and magnetoelastic transitions, and anisotropic magnetostriction in the Mn$_{1.95}$Cr$_{0.05}$Sb single crystal, J. Mag. Magn. Mater. 487 (2019) 165315.

[22] B.H. Toby, Rfactors in Rietveld analysis: how good is good enough, Powder Diffr. 21 (2006) 67–70.

[23] W.H. Cloud, H.S. Jarrett, A.E. Austin, E. Adelson, Neutron diffraction studies of chromium-modified Mn$_2$Sb, Phys. Rev. 120 (1960) 1969–1970.

[24] Y. Zhang, Z. Zhang, Metamagnetic-transition-induced giant magnetoresistance in Mn$_2$Sb$_{1-x}$Sn$_x$ (0 < x ≤ 0.4) compounds, Phys. Rev. B 67 (2003) 132405.

[25] A. Tekgül, Ö. Çakır, M. Acet, M. Farle, N. Ünal, The structural, magnetic, and magnetocaloric properties of In-doped Mn$_{2-x}$Cr$_x$Sb, J. Appl. Phys. 118 (2015) 153903.